Proceedings of the 5th International Conference on Nonlinear Dynamics
ND-KhPI2016
September 27-30, 2016, Kharkov, Ukraine

Simulation of Vibro-Impact Systems Using Reciprocal Mass Matrices

Anton Tkachuk[1]*, Manfred Bischoff[1]

Abstract
Computation cost of explicit time integration can be reduced substantially using the reciprocal mass matrices. General variational derivation of the method, its verification by an eigenvalue benchmark and comparison on a transient example are presented in this contribution.

Keywords
Reciprocal mass matrix, Selective mass scaling, Explicit dynamics

[1]Institute for Structural Machanics, University of Stuttgart, Pfaffenwaldring 7, Stuttgart, D-70550, Germany
***Corresponding author**: tkachuk@ibb.uni-stuttgart.de

Introduction

Vibro-impact systems are often simulated using explicit time integration schemes because of their high robustness for non-smooth and highly dynamic processes and ability to resolve propagation of shock waves. At the same time, these schemes are only conditionally stable resulting in small critical time step and high computational cost for a simulation. In this contribution, a method for increasing of the critical time step with respect to standard lumped mass matrices is presented and a possibility of on application an example of simplified o pneumatic hammers is shown.

A reciprocal mass matrix is the inverse of mass matrix. The lumped (diagonalized) mass matrix yields a diagonal reciprocal mass matrix. The consistent mass matrix yields a fully populated (dense) reciprocal mass, which is impractical. Recently, a variational method for construction of sparse and consistent reciprocal mass matrices was proposed for general finite elements [1]. This method is based on a parametrized variational principle with independent field for displacement, velocity and linear momentum. Choosing an independent discretization of the linear momentum with a local dual basis enables derivation of the sparse reciprocal mass matrix. The free velocity field is condensed on the element level and gives a freedom to tune the dispersion error of the discretization and the critical time step. For an alternative algebraic derivation of the reciprocal mass matrices see [2].

In this contribution, the derivation of reciprocal mass matrices is extended to the total Lagrangian formulation. The correctness of the derivation is illustrated with a standard NAFEMS eigenfrequency benchmark. Potential efficiency of the approach is shown with an example transient simulation of a piston of pneumatic hammer with a brakes. The evolution of stresses at critical points is simulated using lumped mass matrix, reciprocal mass matrix and an algebraic selectively scaled mass matrices of Olovsson [3].

1. Derivation of reciprocal mass matrices

In the following, a unified approach for reciprocal mass matrices based on the modification of the virtual work of d'Alambert force is presented. The concept is verified by a simple eigenvalue benchmark and a transient example.

Starting point for the derivation is the principle of virtual work depending on the single displacement field u_i

$$\delta W(u_i) = \delta W^{\text{int}} + \delta W^{\text{kin}} - \delta W^{\text{ext}}, \tag{1}$$

where the internal, kinetic and external virtual work is defined as

$$\delta W^{\text{int}} = \int_{\Omega} \delta u_{i,j} P_{ij}(\mathbf{F}) \, \mathrm{d}V, \tag{2}$$

$$\delta W^{\text{kin}} = \int_{\Omega} \delta u_i \rho \ddot{u}_i \, \mathrm{d}V, \tag{3}$$

$$\delta W^{\text{ext}} = \int_{\Omega} \delta u_i \rho \hat{b}_i \, \mathrm{d}V + \int_{\Gamma_t} \delta u_i \hat{t}_i \, \mathrm{d}A. \tag{4}$$

Above, $P_{ij}(\mathbf{F})$ is the 1st Piola-Kirchhoff stress computed from the deformation gradient $F_{ij} = \delta_{ij} + u_{i,j}$. $\hat{t}_i$ denotes the traction on the part of the surface Γ_t and $\hat{b}_i$ denotes the body load. The core idea is to modify the virtual kinetic work δW^{kin} by using the variational templates

$$\delta W^{\text{kin},\circ} = \int_{\Omega} \left(\delta p_i \left(\dot{u}_i - (1 - C_2) \rho^{-1} p_i - C_2 v_i \right) - C_2 \delta v_i (p_i - \rho v_i) - \delta u_i \dot{p}_i \right) \mathrm{d}V, \tag{5}$$

with v_i and p_i being the velocity and the linear momentum, C_2 being a free template parameters for the inertia scaling.

Now the modified virtual work expression $\delta W^{\text{kin},\circ}$ is discretized to obtain the equation of motion with selectively scaled inertia. The discretization of the virtual kinetic work $\delta W^{\text{kin},\circ}$ follows the author's paper [1] and yields a sparse variationally selectively scaled sparse reciprocal mass matrix.

The weak form (5) can be discretized using a Bubnov-Galerkin approach with independent discretization for the displacement, velocity and linear momentum

$$u_i \approx u_i^h = \sum_{I=1}^{N_n} N_I u_{Ii}, \qquad \delta u_i \approx \delta u_i^h = \sum_{I=1}^{N_n} N_I \delta u_{Ii}, \tag{6}$$

$$p_i \approx p_i^h = \sum_{I=1}^{N_n} \chi_I p_{Ii}, \qquad \delta p_i \approx \delta p_i^h = \sum_{I=1}^{N_n} \chi_I \delta p_{Ii}, \tag{7}$$

$$v_i \approx v_i^h = \sum_{e=1}^{N_e} \sum_{k=1}^{N_{ve}} \psi_{ik}^{(e)} v_k^{(e)}, \qquad \delta v_i \approx \delta v_i^h = \sum_{e=1}^{N_e} \sum_{k=1}^{N_{ve}} \psi_{ik}^{(e)} \delta v_k^{(e)}, \tag{8}$$

with N_I and χ_I being the shape functions for the displacement and the linear momentum at the I^{th} node and $\psi_{ik}^{(e)}$ being an element-wise interpolation of the velocity. The discretized virtual kinetic work is then

$$\begin{aligned} \delta W^{\text{kin},\circ,h} = \int_{\Omega^h} \big(& \delta p_{Ii} \chi_I \left(N_J \dot{u}_{Ji} - (1 - C_2) \rho^{-1} \chi_J p_{Ji} - C_2 \psi_{ik}^e v_k^e \right) - \\ & - C_2 \psi_{ik}^e \delta v_k^e (\chi_I p_{Ii} - \rho \psi_{il}^e v_l^e) - \delta u_{Ii} N_I \chi_J \dot{p}_{Ji} \big) \, \mathrm{d}V. \end{aligned} \tag{9}$$

Bi-orthogonality of the displacement and momentum shape functions is adopted with

$$\delta_{IJ} = \int_{\Omega^h} \chi_J N_I \, \mathrm{d}V, \tag{10}$$

where δ_{IJ} is the Kronecker-delta. The discretized virtual kinetic work yields two equations

$$\dot{u}_{Ii} = (1 - C_2) C_{IJ} p_{Ji} + C_2 W_{Iik}^{(e)} v_k^{(e)}, \qquad Y_{kl}^{(e)} v_l^{(e)} = W_{Iik}^{(e)} p_{Ii} \tag{11}$$

and additionally a contribution $\dot{p}_{Ii}$ to the equilibrium. The matrices C_{IJ}, $Y_{kl}^{(e)}$ and $W_{Iik}^{(e)}$ are defined as

$$C_{IJ} = \int_{\Omega_e^h} \rho^{-1} \chi_I \chi_J \, \mathrm{d}V, \qquad Y_{kl}^{(e)} = \int_{\Omega_e^h} \rho \psi_{ik}^{(e)} \psi_{ik}^{(e)} \, \mathrm{d}V, \qquad W_{Iik}^{(e)} = \int_{\Omega_e^h} \chi_I \psi_{ik}^{(e)} \, \mathrm{d}V. \tag{12}$$

Eliminating the velocity parameters from (11) yields

$$\dot{u}_{Ii} = C_{IJij}^{\circ} p_{Jj}, \tag{13}$$

where C°_{IJij} is the variationally selectively scaled reciprocal mass matrix (VSRMM) with free parameter C_2

$$C^{\circ}_{IJij} = (1-C_2)C_{IJ}\delta_{ij} + \sum_{e \text{ adjacent to } I,J} C_2 W^{(e)}_{Iik}((Y^{(e)})^{-1})_{kl} W^{(e)}_{Jjk}. \tag{14}$$

Note, that the matrix above stay positive definite for $-1 < C_2 < 1$. From the experience, values close to 1 provide good accuracy and sufficient reduction of the critical time step with respect to lumped mass matrix. The physical dimension of individual entries of the reciprocal mass matrix is kg^{-1}, i.e. the inverse of mass.

Finally, the equation of motion is

$$\dot{p}_{Ii} = f^{\text{ext}}_{Ii} - f^{\text{int}}_{Ii} \tag{15}$$

$$\dot{u}_{Ii} = C^{\circ}_{IJij} p_{Jj}, \tag{16}$$

with the external force vector $f^{\text{ext}}_{Ii} = \int_{\Omega^h} N_I \rho b_i \,\mathrm{d}V + \int_{\Gamma^h_t} N_I t_i \,\mathrm{d}A$ and internal force vectors $f^{\text{int},(e)}_{Ii} = \int_{\Omega^h_e} N_{I,j} \mathbf{P}_{ij} \,\mathrm{d}V$. In geometrically linear case, the internal force is computed $f^{\text{int},(e)}_{Ii} = K_{IiJj} u_{Jj}$, with $\mathbf{K}$ being the stiffness matrix.

2. FV32 benchmark

The derivation of the reciprocal mass matrix seems to be artificial and redundant. In order to illustrate that the reciprocal mass matrix can represent correct inertia properties of a structure, a standard NAFEMS FV32 benchmark is considered. It shows that the lowest structurally relevant eigenfrequencies and eigenmodes are computed with sufficient accuracy and the highest frequency is reduced significantly with respect to the lumped mass matrix.

The setup of the NAFEMS FV32 benchmark is given in Figure 1. It represents a tapered plate made of homogeneous material fixed in both directions at the wide end. In-plane eigenvibration are considered and the reference values for the six lowest modes are provided, see Table 1. Here, this problem is solved using 3-node constant strain triangle elements with a mapped mesh 40×20. The stiffness of the elements is computed exactly using 1-point quadrature. All element mass matrices are computed using three-point quadrature, see e.g. [4]. The default NAG eigenvalue solver is used for the computation of the eigenvalue problem within a Maple implementation of the problem.

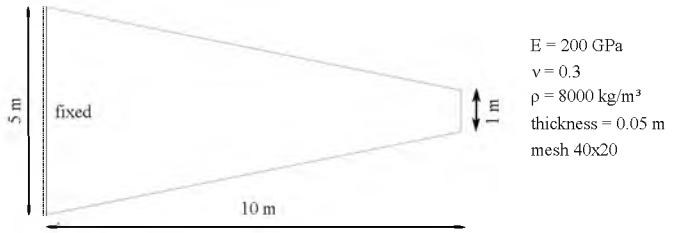

Figure 1. Setup of FV32 NAFEMS benchmark.

	f_1, Hz	f_2, Hz	f_3, Hz	f_4, Hz	f_5, Hz	f_6, Hz	$f_{\max}$, Hz	$f^{\circ}_{\max}/f^{\text{LMM}}_{\max}$
Reference	44.623	130.03	162.70	246.05	379.90	391.44	-	-
CMM	44.845	130.94	162.75	248.46	384.73	391.91	65795	1.72
LMM	44.825	130.70	162.71	247.47	382.00	391.25	37125	1.00
VSRMM, $C_2 = 0.99$	44.799	130.37	162.66	246.12	378.26	390.66	19172	0.52

Table 1. Six lowest frequencies for FV32 benchmark computed with consistent, lumped and reciprocal mass matrix. Mesh: 40×20 elements.

Computation of the reciprocal mass matrix requires a bi-orthogonal basis to satisfy the bi-orthogonality condition (10). Here, a close form expressions for the dual base from [5] are used with

$$N_1 = 1-\xi-\eta \qquad N_2 = \xi \qquad N_3 = \eta, \tag{17}$$

$$\chi_1 = 3-4\xi-4\eta \qquad \chi_2 = 4\xi-1 \qquad \chi_3 = 4\eta-1. \tag{18}$$

The constant element-wise ansatz for the velocity shape functions is used

$$\psi_{ik}^{(e)} = \begin{bmatrix} 1 & 0 \\ 0 & 1 \end{bmatrix} \tag{19}$$

The eigenmodes and eigenfrequencies in cas of the reciprocal mass matrix are computed from eigenvalue problem as follows

$$(\mathbf{C}^{\circ}\mathbf{K} - \omega^2\mathbf{I})\phi = \mathbf{0}. \tag{20}$$

The six lowest eigenfrequencies computed with consistent, lumped, and variationally scaled reciprocal mass matrix are given in Table 1. The relative error for consistent mass matrix for the six lowest modes is 1.2% whereas for lumped and VSRMM is below 0.6%. At the same time, the reciprocal mass matrix provides 48% reduction of the highest frequency with respect to lumped mass matrix, e.g. the critical time step for the alternative discretization is almost twice higher.

The six lowest eigenmodes computed with VSRMM are shown in Figure 2. They are visually similar to the given in the benchmark sheet.

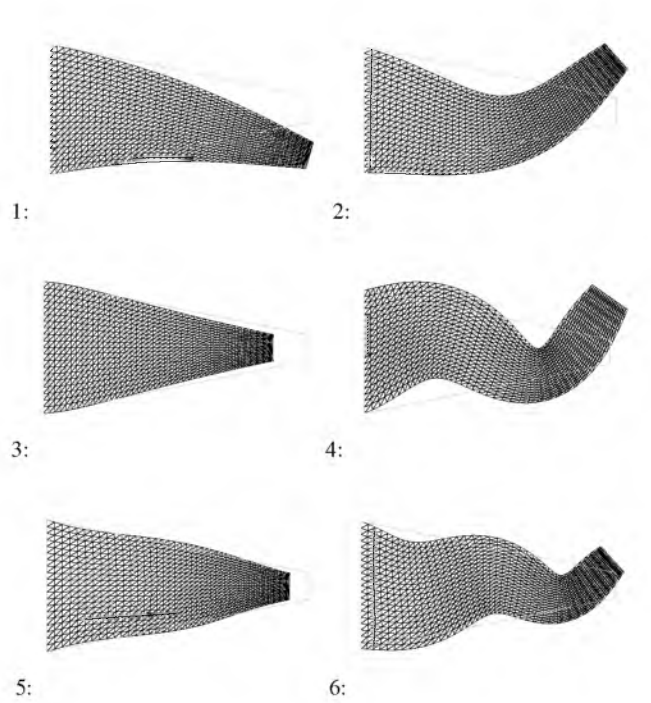

Figure 2. The six lowest modes for FV32 NAFEMS benchmark computed with T1 element and variationally scaled reciprocal mass matrix with $C_2 = 0.99$. Mesh: 40×20 elements. The gray polygon represents edges of the undeformed structure.

3. Transient example for a simplified hammer model

Possibility of application of reciprocal mass matrices to vibro-impact system is shown here on example of pulse load on a piston of a pneumatic hammer with brakes. Consider a two-dimensional simplified model of hammer in Figure 3. The piston of the hammer consists of an elongated rod, thick head and connection to rubber-metallic brake. The brake connects the piston to the housing. Both parts are assumed to be elastic and isotropic with properties given in the Figure 3. Connection to housing is assumed to be perfect clamping. The piston is subjected to pulse pressure loading at thin end in first 20 mks as $p = 0.005(1+\cos(100\pi t))$, GPa. The response of the hammer is simulated for the first 100 mks. A normal stress component σ_{xx} at point A (before brake) and B (after brake and before head) are the target values.

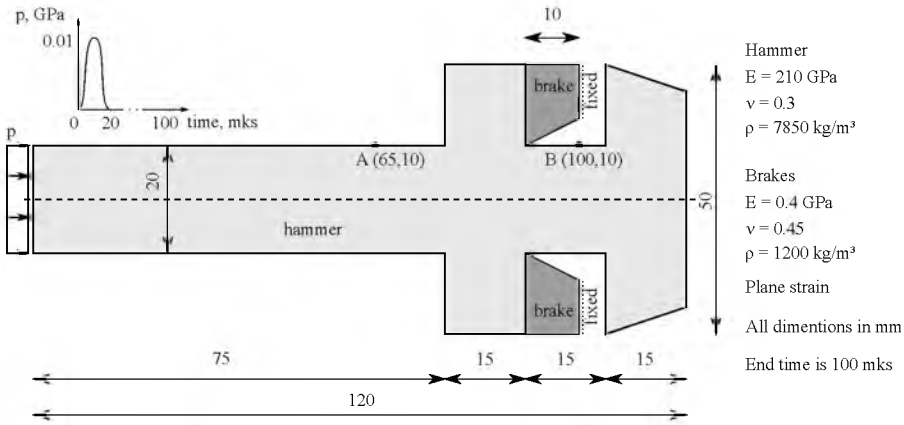

Figure 3. Setup for simplified hammer example.

The piston and the brakes are discretized using 4-node fully integrated quadrilateral finite elements with two displacement per node and with average element size 1 mm (102 elements per wave-length of loading pulse). This result in a model with 3680 finite elements and 3904 nodes. The time integration is performed using central difference scheme using time step being 90% of the critical value. The critical time step is computed from the highest global eigenfrequency of the system using the forward iteration method, see [6]. The corresponding critical time steps for the lumped mass, selectively scaled reciprocal mass and algebraically selectively scaled mass matrices are given in Table 2. The reciprocal mass matrix is computed for the standard dual basis and the constant basis (19). For all mass scaling methods, the uniform values of mass scaling are used.

Mass type	Δt_{crit}, ns	Δt, ns	Relative cost	Aver. number PCG iter.for $\lvert R\rvert < 10^{-6}$
LMM	109	98.1	1.00	-
VSRMM, $C_2 = 0.83$	126	113.4	0.88	-
VSRMM, $C_2 = 0.95$	198	178.2	0.58	-
ASMS, $\beta = 2.06$	206	185.4	0.67	10
ASMS, $\beta = 4.12$	269	241.1	0.52	13

Table 2. Critical time step and relative cost for the hammer example.

The simulation is performed within NumPro (C++ written in-house finite element code of Institute for Structural Mechanics, University of Stuttgart). This code has implementation of several advances selective mass scaling methods. Algebraic selective mass scaling (ASMS) proposed in [3] is among these methods. This method adds artificial terms to lumped mass matrix on diagonal and off-diagonal terms keeping the translational mass of structure and selectively reducing the highest eigenfrequencies. However, this method results in non-diagonal mass matrix, which requires solution of a linear system for the acceleration vector from the total force vector each time step ($\ddot{\mathbf{u}} = \mathbf{M}^{-1}\mathbf{F}^{\text{tot}}$). This can be efficiently

done using the preconditioned conjugate gradient method with Jacobi preconditioner as proposed in [7]. Usually, PCG requires few iteration to converge, as shown in last column of Table 2, but adds an additional overhead to the mass scaling procedure (about 33% in the considered example). Such overhead is avoided for the reciprocal mass matrices where the inverse is directly provided.

The history of normal stress σ_{xx} at points A and B are given in Figure 4. All proposed mass matrix discretization correctly represent evolution of stress: Arrival time of the stress pulse, negative stress behind the shock wave and arriving reflected pulse. Only ASMS with $\beta = 4.12$ yield slight phase shift. VSRMM with $C_2 = 0.95$ for the same quality of results as lumped mass matrix can save 42% of computational cost, see Table 2. Using smaller values of C_2, e.g. 0.83 , yield less speed up and it is not advised.

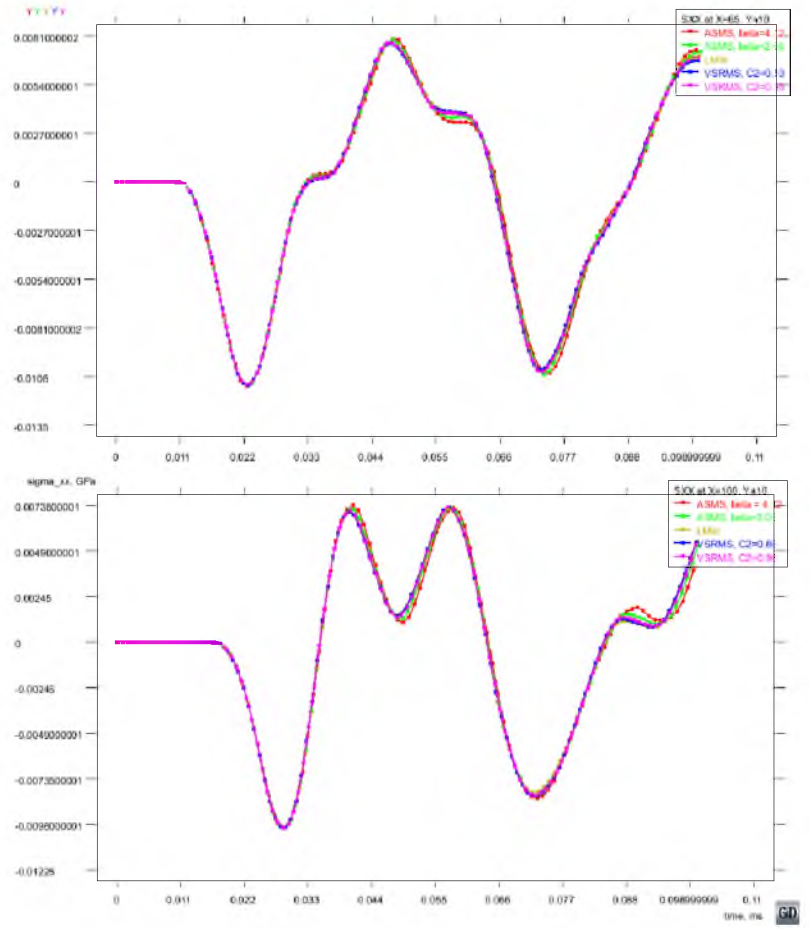

Figure 4. Evolution of xx component of Cauchy stress at point A (above) and B (below).

Conclusions

Reciprocal mass matrices can represent complicated dynamic behavior and reduce the computational cost of explicit time integration. Variational derivation of the reciprocal mass matrices uses the parametrized principle of virtual work with free velocity and linear momentum fields. For a space form of the reciprocal mass matrix the dual basis for linear momentum and an element-wise base for velocity must be used. Reduction of computational cost in range 42-48% is obtained for the examples above.

Direction of future research

The given example and theory is not yet sufficient to cover all needs. The future steps are implementation of penalty contact, local (nodal) time step estimate and finding the optimal values of coefficient C_2 for wide range of finite elements. This research is foreseen in project BI 722-8/1 "Variational methods for mass scaling" funded by German Research Foundation.

Acknowledgments

Fruitful discussions of selective mass scaling and reciprocal mass matrices with Anne Schäuble, Lionel Morancay, Gérard Winkelmuller, and Radek Kolman are gratefully acknowledged. The authors would also like to thank the Baden-Württemberg Stiftung gGmbH, for funding HPC-10 project. The initial idea of variational mass scaling was developed withing HPC-10 project.

References

[1] Tkachuk A, Bischoff M. Direct and sparse construction of consistent inverse mass matrices: general variational formulation and application to selective mass scaling. International Journal for Numerical Methods in Engineering. 2015;101(6):435–469.

[2] Lombardo M, Askes H. Lumped mass finite element implementation of continuum theories with micro-inertia. International Journal for Numerical Methods in Engineering. 2013;96(7):448–466.

[3] Olovsson L, Simonsson K, Unosson M. Selective mass scaling for explicit finite element analyses. International Journal for Numerical Methods in Engineering. 2005;63(10):1436–1445.

[4] Zienkiewicz OC, Taylor RL. The Finite Element Method Set. 6th ed. Amsterdam: Elsevier/Butterworth-Heinemann; 2006.

[5] Lamichhane BP, McBride A, Reddy B. A finite element method for a three-field formulation of linear elasticity based on biorthogonal systems. Computer Methods in Applied Mechanics and Engineering. 2013;258:109–117.

[6] Benson DJ, Bazilevs Y, Hsu MC, Hughes TJR. Isogeometric shell analysis: The Reissner-Mindlin shell. Computer Methods in Applied Mechanics and Engineering. 2010;199(58):276 – 289.

[7] Olovsson L, Simonsson K. Iterative solution technique in selective mass scaling. Communications in Nummerical Methods in Engineering. 2006;22(1):77–82.